Nanoscale

ROYAL SOCIETY OF CHEMISTRY

PAPER

View Article Online
View Journal | View Issue

Cite this: *Nanoscale*, 2025, **17**, 10752

P(TT-TPA) featuring a conjugated extended structure: enabling high-performance flexible electrochromic-supercapacitors†

Jiaming Li,‡[a] Xu Cheng,‡[b] Chunhui Du,[c] Wanyi Zhang,[c] Li Sheng,[b] Wenyuan Xu,[a] Hui Shi,[a] Ge Zhang *[c] and Xubiao Luo*[a]

Electrochromic-supercapacitors (EC-SCs) based on conducting polymers hold broad application prospects in fields such as smart electronic devices, wearable devices, and the Internet of Things. However, complex structures generated by their large molecular weights severely deteriorate the disorder of chain arrangements, which significantly hinders the migration of charge carriers within the chains and exerts an adverse impact on the opto/electric performance. In this work, triphenylamine (TPA) is adopted as the scaffold, and thieno[3,2-*b*]thiophene (TT) groups are introduced to successfully construct TT-TPA (HTPA) with a conjugated extended structure. Leveraging the intermolecular π–π stacking effect effectively restricted the rotation of single bonds, significantly enhancing the molecular planarity. Concurrently, the introduction of multiple active sites opened up more channels for charge storage. The obtained P(TT-TPA) (**PHTPA**) films exhibit remarkable optical contrast (51% at 1050 nm) and outstanding energy storage capacity (177 F g^{-1} at 1 A g^{-1}). The flexible devices based on **PHTPA** show significant color changes, excellent capacitive performance (46 F g^{-1} at 1 A g^{-1}), and good bending resistance. In summary, the molecular design strategy of expanding the conjugated structure furnishes a certain theoretical foundation and referential significance for the development of EC-SC electrode materials that balance comprehensive performances.

Received 20th January 2025,
Accepted 26th March 2025

DOI: 10.1039/d5nr00272a

rsc.li/nanoscale

1. Introduction

Supercapacitors, owing to their rapid charge and discharge speed, high energy density and excellent safety performance, have precisely filled the performance gap between traditional capacitors and batteries.[1,2] As one of the novel energy storage devices, they have attracted widespread attention. In recent years, the market demand for micro-energy storage devices has expanded particularly due to the rapid advancement of artificial intelligence, which has propelled the research and innovation of diverse new energy storage technologies.[3] Thus, the development and research of multifunctional energy storage devices are proceeding in full swing. Among them, electrochromic supercapacitors (EC-SCs), as cutting-edge multifunctional devices, feature an innovative integrated architecture that combines optical signal modulation and high-efficiency energy storage.[4,5] This breakthrough overcomes the limitation of single-function in traditional devices. The characteristic that the energy storage state and color change are synchronized in real-time exhibits huge application prospects in self-powered rescue displays,[6,7] wearable health monitoring devices[8,9] and consumer electronics.[10] However, the development of EC-SCs that can concurrently balance electrochromic performance and capacitive performance remains an enduring challenge.[11,12]

In EC-SCs, electrodes that simultaneously exert electrochromic and energy storage functions are their crucial components. Conducting polymers (CPs) have been demonstrated to be suitable for use as electrode materials of EC-SCs due to their favorable redox activity, adjustable molecular structures, and facile processability.[13–15] The orderliness of molecular chain packing determines the aggregated state structure of polymers to a large extent,[16] and plays a crucial role in the transmission efficiency and pathways of the intra-chain carriers.[17] It exerts a profound impact on the electron transport efficiency of CPs and ultimately has a direct bearing on the electrochemical properties of the electrode materials.[18]

[a]*Key Laboratory of Jiangxi Province for Persistent Pollutants Prevention Control and Resource Reuse, Nanchang Hangkong University, Nanchang, 330063, P. R. China. E-mail: luoxubiao@126.com*
[b]*College of Chemistry and Chemical Engineering, Jiangxi Science & Technology Normal University, Nanchang 330013, Jiangxi, P. R. China*
[c]*Jiangxi Provincial Key Laboratory of Flexible Electronics, Flexible Electronics Innovation Institute, Jiangxi Science & Technology Normal University, Nanchang 330013, Jiangxi, P. R. China. E-mail: zhangge20082006@126.com*

†Electronic supplementary information (ESI) available. See DOI: https://doi.org/10.1039/d5nr00272a

‡These authors contributed equally to this work.

Nevertheless, CPs generally possess relatively large molecular weights and manifest complex molecular architectures.[19,20] The lack of periodicity in the inter-chain arrangement gives rise to the localization of charge carriers, thereby exacerbating the difficulty of their transportation within the material.[21] This not only decelerates the color-changing speed and reduces the efficiency but also poses obstacles to ion storage, impeding the enhancement of capacitive performance.[22,23] Therefore, it is highly worthy to explore ways to utilize weak intermolecular forces like π–π stacking from the microscopic aspect of molecular design to regulate the aggregate state structure of polymer molecules and achieve concurrent improvement in both electrochromic and capacitive properties.

In this work, we put forward a strategy for expanding the conjugated backbone structure of CPs to facilitate the formation of π–π stacking by introducing thieno[3,2-*b*]thiophene (TT) groups with triphenylamine (TPA) as the backbone. The incorporation of TT extends the planar conjugated backbone of TPA derivatives, while simultaneously furnishing more active storage sites for conductive ions. Based on this, the conducting monomer TT-TPA (HTPA) was designed and synthesized *via* the Stille coupling reaction. P(TT-TPA) (**PHTPA**) prepared by electropolymerization in the boron trifluoride diethyl etherate (BFEE) system exhibits excellent electrochromic properties (with a transmittance of 51% at 1050 nm), satisfactory mass-specific capacitance (177 F g^{-1} at 1 A g^{-1}), and remarkable rate performance (with only a 9% capacitance decay when the current density increases from 1 to 10 A g^{-1}). A flexible asymmetric EC-SC device based on **PHTPA** possesses a considerable optical contrast (20% at 570 nm), outstanding mass-specific capacitance (46 F g^{-1} at 1 A g^{-1}), and remarkable cycling stability (with 75% of the capacitance remaining after 3000 cycles). It is discovered that the device exhibits excellent bending resistance (with a capacitance retention rate of 80% at a 180° bend and a mere 20% transmittance decay after 200 bends).

2. Experimental section

2.1 Chemicals and materials

Tris(4-bromophenyl)amine (98%, Adamas), tributyl(thieno[3,2-*b*]thiophen-2-yl)stannane (98%, Bidepharm), tetrakis(triphenylphosphine)palladium ($Pd(pph_3)_4$, 99%, J&K), tetrahydrofuran (THF, AR, Aladdin), BFEE (98%, Aladdin), EDOT (99%, Aladdin), acetonitrile (ACN, AR, J&K), dichloromethane (DCM, 99.9%, Aladdin), poly(methyl methacrylate) (PMMA, 98%, Energy Chemistry), propylene carbonate (PC, GC, J&K), indium tin oxide coated (ITO) PET film (ITO-PET, sheet resistance: 30–35 Ω sq^{-1}, Zhuhai Kaivo), and ITO glass (sheet resistance < 10 Ω sq^{-1}, Zhuhai Kaivo) were purchased and used without further purification. Lithium perchlorate ($LiClO_4$, 98%, Energy Chemistry) was vacuum dried at 65 °C for 12 h before use.

2.2 The synthesis of monomers

300 mg of tris(4-bromophenyl)amine (0.62239 mmol) was dissolved in 210 mL of THF, and 1.07 g of tributyl(thieno[3,2-*b*]thiophen-2-yl)stannane (2.49 mmol) was added. Then 215.77 mg of $Pd(PPh_3)_4$ (0.18672 mmol) was added as a catalyst. After stirring until it was completely dissolved, the mixture was stirred for 24 h under the protection of N_2, and a brown oily product was obtained. The product was purified through processes such as extraction with a separatory funnel, purification by column chromatography and vacuum distillation. As a result, 131 mg of a pale yellow solid was obtained in a yield of 31.89%. ^{1}H NMR (400 MHz, $CDCl_3$), δ 7.55 (d, J = 8.5 Hz, 2H), δ 7.43 (s, 1H), δ 7.35 (d, J = 5.2 Hz, 1H), 7.24 (d, J = 5.2 Hz, 1H), 7.18 (d, J = 8.5 Hz, 2H).

2.3 Electropolymerization and electrochemical testing

Both the polymerization process and the electrochemical tests were conducted within a three-electrode system. A self-made Ag/AgCl reference electrode was obtained by the potentiostatic electrodeposition of an Ag wire with a diameter of 1 mm in a 6 M HCl solution at a constant potential of 1.5 V for 100 s. The chemically inert Pt wire (with a diameter of 1 mm) served as the auxiliary electrode, while the ITO glass with an effective area of 0.7 cm × 1.5 cm or the ITO-PET with a size of 2.5 cm × 3 cm was employed as the working electrode. In order to achieve the optimal electrochromic and energy storage performances, **PHTPA** films with different thicknesses were obtained by electrodepositing in a BFEE solution containing 0.01 M monomer at a constant potential of 1 V for varying durations. Subsequently, the surfaces of the films were rinsed with ACN to remove the residual monomer and BFEE. The **PHTPA** film attached to the ITO substrate was utilized as the working electrode, and a series of electrochemical tests were carried out in monomer-free BFEE by employing the aforementioned three-electrode system.

2.4. Construction of PHTPA//PEDOT-based flexible EC-SCs

The EC-SC device adopts a sandwich structure, which comprises the conductive layer, cathode, anode and electrolyte. The **PHTPA**/ITO-PET electrode serves as both the conductive layer and the anode simultaneously, while the PEDOT/ITO-PET electrode functions as both the conductive layer and the cathode at the same time. An appropriate amount of gel electrolyte was coated onto the cathode and the anode, respectively, with the assistance of double-sided adhesive tape, which adhered them together. Organic glue was applied around the ITO-PET to prevent the leakage of the electrolyte. After allowing it to air-dry naturally for 30 minutes until it solidified, it could be used for testing. The gel electrolytes were prepared by stirring $LiClO_4$, ACN, PMMA, and PC in a mass ratio of 3 : 70 : 7 : 20 at 60 °C for 8 h under N_2 protection.

3. Results and discussion

3.1. The molecular design strategy for conjugated extended structures

TPA, as one of the representative substances, features an electron-rich structure composed of N atoms and benzene rings,

which gives rise to a delocalized electron system with an even broader conjugated range. Moreover, the nearly planar molecular configuration of TPA facilitates π–π stacking among molecules. These characteristics endow TPA with excellent hole-transporting capabilities,[24–26] thereby rendering it widely used in electrode materials of EC-SCs (Fig. 1a). Based on this, we designed conjugated extended structures to facilitate the formation of π–π stacking, and then regulate the morphological structures of polymers (Fig. 1b), thereby enhancing their electrochemical properties. The utilization of TPA and TT (Fig. 1c) as basic constituent units primarily stems from the following considerations: (1) the quasi-planar molecular configuration of TPA,[27] in combination with planar TT,[28,29] allows for an interaction between their π-electrons. This interaction engenders a substantially larger delocalized electron system, thereby precipitating a notable expansion of the conjugated structure. This not only enhances the rigidity of the molecular chains but also restricts the free rotation and bending between chains, thus facilitating a more regular arrangement and extended state among the molecular chains. Moreover, the π–π stacking interactions between molecules become more prominent, compelling the molecular chains to align in a specific manner. The ordered arrangement among molecular chains provides more direct and efficient pathways for electron transmission. While meeting the requirement of rapid insertion and extraction of ions during the electrochromic process, it also exerts a positive influence on the rate performance of the capacitor. (2) The introduction of TT units furnishes the TPA backbone with more active sites. TPA and TT can participate in redox reactions during the charge–discharge process, and this dual-capacitance storage mechanism is capable of significantly enhancing the specific capacitance of the material. In conclusion, the molecular design strategy of expanding the conjugated structure holds the promise of simultaneously elevating

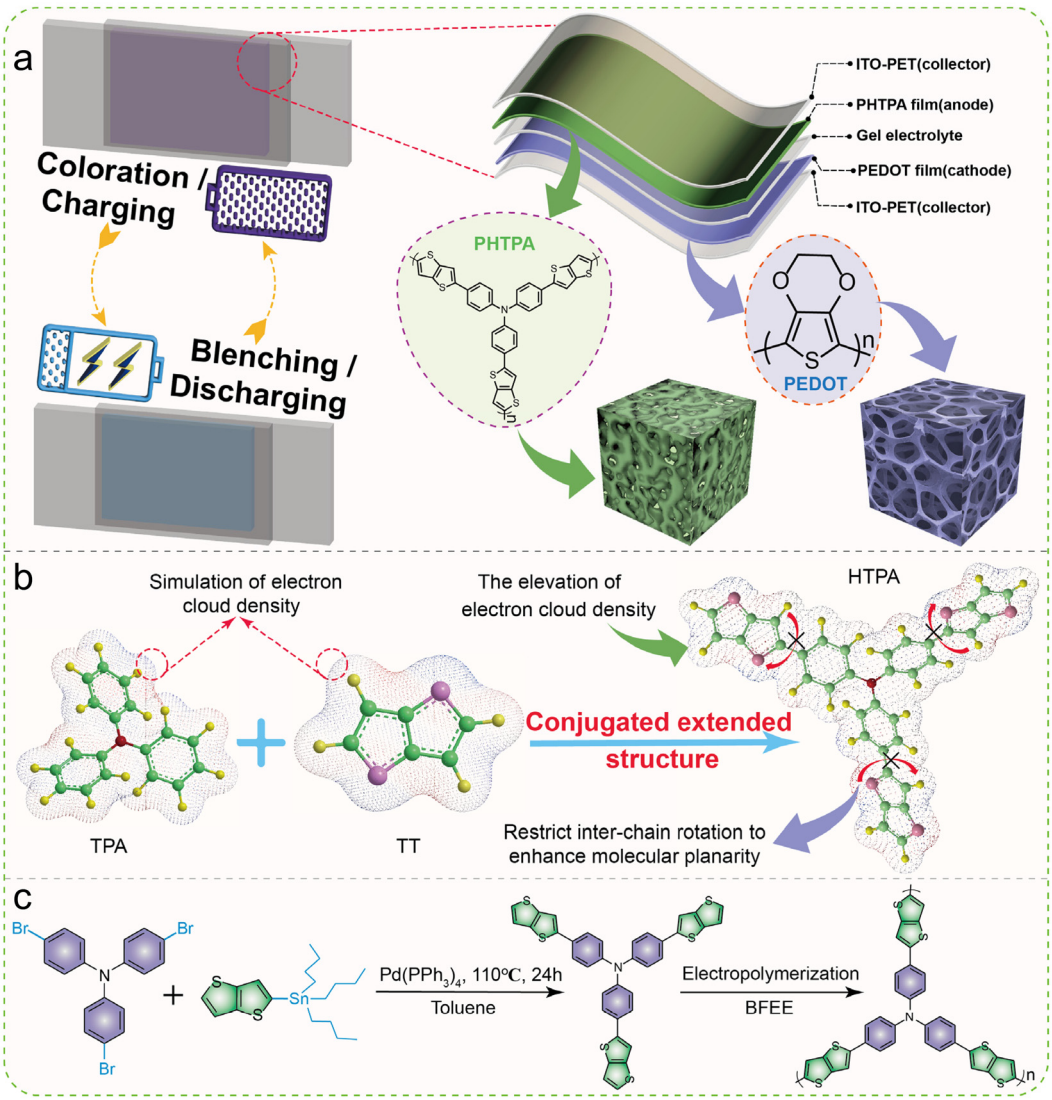

Fig. 1 (a) Conceptual diagram and application scenarios of **PHTPA**//PEDOT-based flexible devices. (b) The design strategy of conjugated extended structures. (c) The synthesis pathway of HTPA molecules.

the electrochromic performance as well as the capacitive performance.

3.2. Characterization of PHTPA structures and morphologies

The B3LYP generalized density-functional theory was used for structural optimization and energy-level orbital calculations to characterize the optical and electrical properties (Fig. 2a). The HTPA molecule has a band gap of 3.39 eV, which is far smaller than that of bithiophene (4.62 eV) and TPA (5.12 eV). Its light absorption threshold wavelengths are around 365 nm, 268 nm, and 242 nm respectively. The wavelength of 365 nm lies on the absorption edge of ultraviolet light. HTPA may present a blue-green color (while at the wavelengths of 268 nm and 242 nm, it is transparent or colorless). Under the impetus of voltage, more conspicuous color changes will be manifested. Furthermore, a smaller band gap indicates lower transition energy and usually comes with a higher carrier concentration, which is conducive to the enhancement of electrical conductivity. In order to explore the disparities between the polymer and monomer structures, the infrared spectra of both were tested (Fig. 2b). Peaks in the range of 500–800 cm^{-1} are ascribed to stretching vibrations of C–S bonds in the bithiophene ring (at 548 cm^{-1}, 726 cm^{-1}, and 824 cm^{-1}). Peaks from 1100–1350 cm^{-1} are induced by stretching vibrations of C–N bonds (at 1118 cm^{-1} and 1322 cm^{-1}). Peaks within 1400–1600 cm^{-1} are attributed to stretching vibrations of C=C bonds in the benzene ring and the thiophene ring (at 1418 cm^{-1} and 1637 cm^{-1}). The peak at 3059 cm^{-1} is assigned to the stretching vibration of unsaturated C–H bonds. It is noteworthy that, compared with monomers, the increased conjugation degree of polymers leads to significant changes in the position, absorption intensity and peak width of absorption peaks. For instance, the absorption peak of the polymer at 3054 cm^{-1} witnesses an increase in the dipole moment due to conjugation, which results in the enhancement of the absorption peak intensity. The absorption peak at 1488 cm^{-1} also undergoes a red shift caused by the increase in the conjugation degree. Furthermore, the polymeric structure may introduce new vibration modes or split the originally degenerate vibration modes, thereby resulting in an increase in the number of absorption peaks (the number of absorption peaks within the range of 1100–1350 cm^{-1} changes from two to three). The ultraviolet absorption spectrum also exhibits the above-mentioned phenomenon (Fig. 2c). The ultraviolet absorption of the polymer undergoes a red shift compared with that of the monomer (the absorption peak changes from 368 nm to 416 nm), and the absorption peak becomes broader, which may be related to the diversification of the polymer's energy level distribution. The aggregated state structure and surface morphology of the **PHTPA** film were observed by means of scanning electron microscopy (Fig. 2d). This structure exhibits a relatively regular granular morphology. There exists a certain agglomeration phenomenon among the granules, which leads to the formation of structures similar to chain-like or cluster-like ones. Such agglomeration may be caused by interactions like π–π stacking among polymer molecules. Moreover, the surfaces of the granules possess a certain degree of roughness, which may provide more active sites con-

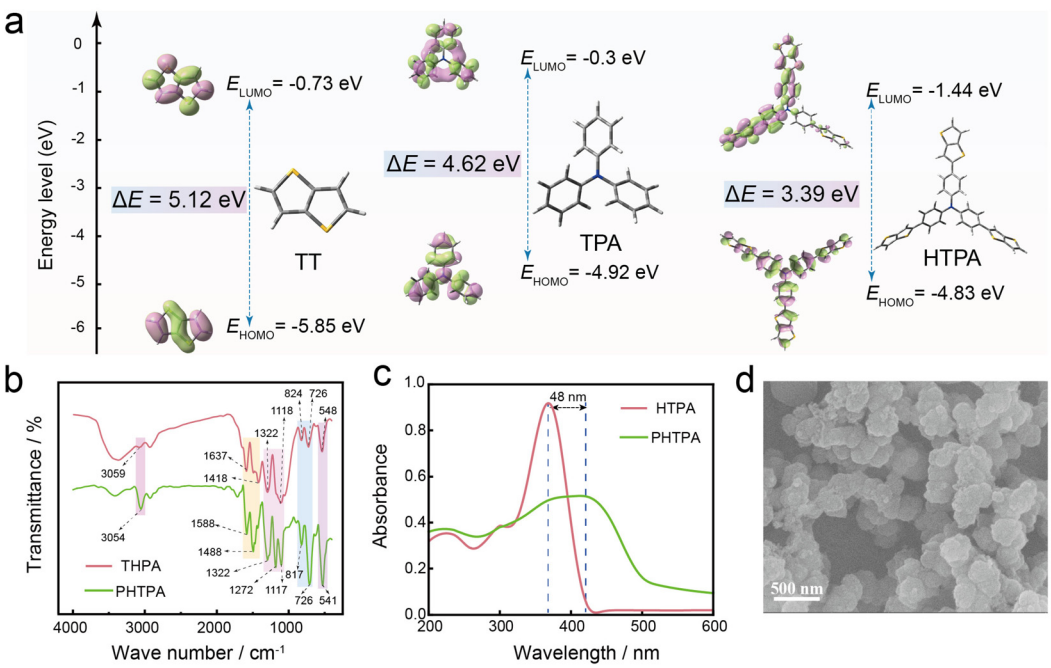

Fig. 2 Theoretical calculations, structural and morphological characterization of HTPA molecules. (a) Calculation of molecular orbital energies and band gaps of TT, TPA and HTPA using the density functional theory. (b) Comparison of infrared spectra of **PHTPA** and HTPA. (c) Comparison of infrared spectra of **PHTPA** and HTPA. (d) SEM images of **PHTPA**.

ducive to the enhancement of capacitive performance. In addition, we conducted SEM characterization of the cross-section of the **PHTPA** material (Fig. S1†) and measured the film thickness (Fig. S2†). The cross-sectional SEM images reveal that the material is composed of tightly packed micrometer-sized particles with rough surfaces and uniform distribution, exhibiting nanoscale protrusions and forming an interconnected three-dimensional network structure. Meanwhile, the thickness of the **PHTPA** film is only 1 μm.

3.3. Electrochemical, capacitive and electrochromic properties of PHTPA films

In the three-electrode system, the linear sweep voltammetry test shows that the oxidation potential of HTPA is as low as 0.2 V, significantly lower than that observed in the ACN system (Fig. S3†). indicating that HTPA possesses excellent electroactivity. The voltage intervals (−0.4 to 1.5 V) and scan rates (100 mV s^{-1}) are set respectively. After 20 cycles of cyclic voltammetry (CV) scanning, the peak currents of redox reactions increase with the increase in the number of cycles (Fig. S4†), successfully achieving the electro-polymerization of **PHTPA**. The **PHTPA** film can also be successfully prepared by linear sweep voltammetry under a constant potential of 0.7 V. All kinds of electrochemical tests were carried out in the BFEE solution without monomers using the three-electrode system. Firstly, the CV curves within the scan rate range from 50 to 300 mV s^{-1} were tested (Fig. 3a). Under the voltage interval ranging from −0.3 V to 1.2 V, the **PHTPA** film exhibits distinct redox peaks at 0.5 V and 0 V. As the scan rate increases, the peak-to-peak separation becomes more pronounced. This may be attributed to the fact that the concentration polarization phenomenon is more severe under high current densities, which will affect the reversibility of the redox reactions of **PHTPA**. To further reveal the kinetic properties of **PHTPA**, the curve depicting the relationship between the peak current density (i) and the scan rate was plotted[30,31] (Fig. S5†). The two curves maintain excellent symmetry, and the current density varies linearly with the voltage, indicating that the electrochemical reactions occurring in **PHTPA** possess a high degree of reversibility. Meanwhile, adsorption control is the rate-determining step of this reaction. Therefore, how to regulate the molecular structure to provide more ion diffusion channels may be one of the keys to improving the electrochemical performance of polymeric materials. The *b* values corresponding

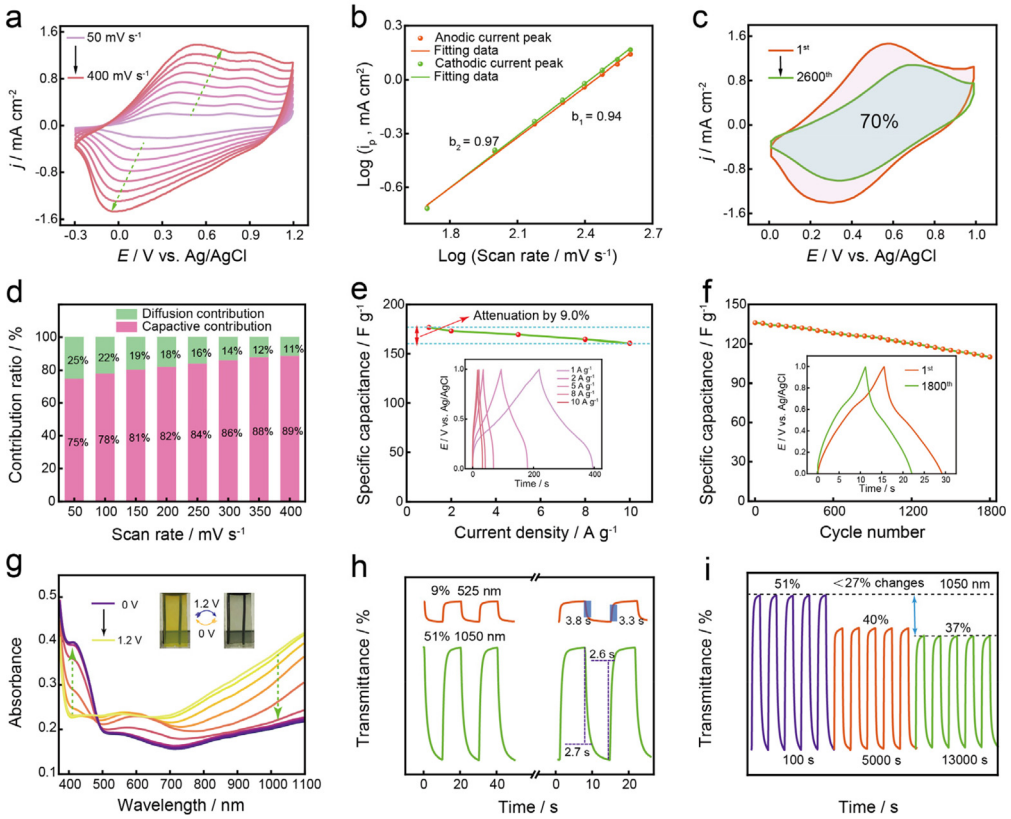

Fig. 3 Electrochemical properties of **PHTPA**. (a) The CVs of **PHTPA** in the BFEE system (scan rate range: 50–400 mV s^{-1}, voltage interval: −0.3–1.2 V). (b) The *b* value was obtained by fitting the peak currents of the cathode and anode with the voltage. (c) **PHTPA** CV stability (at 100 mV s^{-1}). (d) Pseudocapacitance contribution ratio of **PHTPA** (scan rate range: 50–400 mV s^{-1}). (e) Rate performance of the **PHTPA** film, with the inset showing capacitance values at different current densities. (f) Capacitive stability of the **PHTPA** film (at 10 A g^{-1}). (g) Spectroelectrochemical curves of **PHTPA** films (voltage interval: 0–1.2 V). (h) Transmittance values and response times of **PHTPA** films at 525 nm and 1050 nm. (i) Transmittance stability of **PHTPA** films at 1050 nm.

Table 1 Comparison of the response time of **PHTPA** films with those in other works

Absorption wavelength (nm)	Coloration time (s)	Bleaching time (s)	Ref.
525	3.8	3.3	This work
1050	2.7	2.6	
517	4.0	2.8	12
380	3.5	5.5	25
461	5.1	2.3	32
655	3.4	3.38	37
816	10	7	45

to the cathode and anode (the ratio between $\log i$ and $\log v$)[32,33] are calculated to be 0.97 and 0.94 respectively (Fig. 3b), indicating that **PHTPA** has a pseudocapacitive energy storage mechanism. The CV stability of the **PHTPA** film was tested at a scan rate of 100 mV s^{-1} (Fig. 3c). After 2600 cycles, 70% of the active area remained, demonstrating the excellent electrochemical stability of **PHTPA**. Subsequently, the proportions of the diffusion contribution and the capacitive contribution[34,35] at different scan rates were fitted (Fig. 3d). The proportion of the capacitive contribution increases with the increase in the scan rate, indicating that the reactions on the electrode surface rely more on the rapid capacitive process, while the relative contribution of the diffusion process decreases. This draws a similar conclusion to that obtained from the CV curves at different scan rates. The capacitive capability of the **PHTPA** film was tested by chronopotentiometry (CP) (Fig. 3e, inset). **PHTPA** exhibits a high capacitance of 177 F g^{-1} (at a current density of 1 A g^{-1}). The construction of multiple active sites of TPA and TT has a positive impact on its capacitance contribution. The capacitance still reaches 161 F g^{-1} (10 A g^{-1}) with only a 9% attenuation in the capacitance value (Fig. 3e). The excellent rate performance indicates that **PHTPA** can meet the requirements of high-power energy storage devices and is expected to broaden the application scenarios of **PHTPA** as an electrode material. The enhancement of the internal molecular order resulting from the conjugated extended structure may be an important factor in improving the rate performance. The capacitance stability of **PHTPA** was tested (Fig. 3f). After 1800 cycles, 80% of the capacitance was retained. Combining an electrochemical workstation with an ultraviolet-visible spectrophotometer, the spectral absorption curves of **PHTPA** varying with voltage were

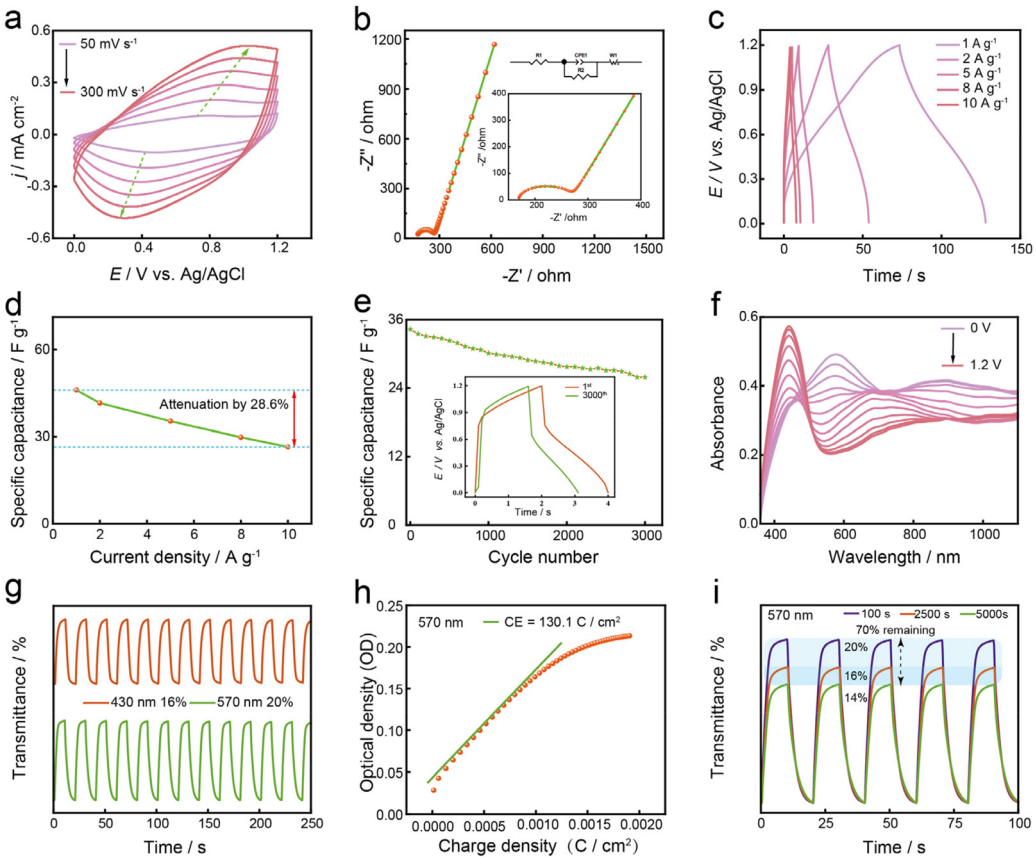

Fig. 4 Electrochemical properties of flexible EC-SCs based on **PHTPA**. (a) The CVs of flexible devices (scan rate range: 50–300 mV s^{-1}, voltage interval: 0–1.2 V). (b) Impedance of flexible devices (open-circuit voltage: 0.229 V, with the inset being the equivalent circuit diagram). (c) Capacitance values of the flexible devices at different current densities. (d) Rate performance of the flexible devices (1 to 10 A g^{-1}). (e) Capacitance stability of the flexible devices (at 20 A g^{-1}). (f) Spectroelectrochemical curves of the devices (voltage interval: 0–1.2 V). (g) Transmittance values at 430 nm and 570 nm. (h) Coloring efficiency of the devices. (i) Transmittance stability of the devices (at 570 nm).

tested within the range of 390 nm to 1100 nm (Fig. 3g). The conjugated structure of **PHTPA** (under the voltage interval from 0 V to 1.2 V) underwent significant changes, resulting in obvious differences in the absorption spectra at 525 nm and 1050 nm (the color of the film changed from yellowish-green to brownish-black). The transmittance switching characteristics of **PHTPA** were tested by chronoamperometry with a pulse time of 10 s (Fig. 3h). The transmittance values at 1050 nm and 525 nm were obtained as 51% and 9% respectively. Moreover, the coloring time and bleaching time required for a 90% change in transmittance[36,37] were calculated to be 2.7 s/2.6 s (at 1050 nm) and 3.8 s/3.3 s (at 525 nm), respectively. When compared with recent works, it demonstrates a moderate response speed (Table 1). The transmittance cycling stability was evaluated (Fig. 3i). After 13 000 s of pulsed voltage cycles, 72.5% of the transmittance remained, indicating fairly good stability. The above test results demonstrate that the **PHTPA** film possesses a high capacitance. Meanwhile, it also exhibits a wide transmittance modulation range. All of these verified the effectiveness of the conjugated structure expansion strategy.

3.4. PHTPA//PEDOT-based flexible EC-SC devices and performance tests

Based on the excellent electrochromic ability and high mass-specific capacitance of the **PHTPA** film, PEDOT was employed as the counter electrode for the flexible EC-SC devices. Furthermore, flexible EC-SC devices based on **PHTPA**//PEDOT with a sandwich structure were assembled. The CV curves of the device under different voltages (voltage range: 0–1.2 V) were tested (Fig. 4a). The intensity of the peak current increased as the scan rate rise, and distinct redox peaks were still observed. The positions and shapes of the peaks at high voltages still maintained a fairly good symmetry, indicating that the electrochemical reactions of the device may possess excellent reversibility. Electrochemical impedance spectroscopy (EIS) was utilized to further evaluate the reaction kinetics of the device (Fig. 4b). A small equivalent series resistance (with R_s being 128.9 Ω) indicates that the internal resistance of the device is relatively low, which is conducive to reducing the energy loss during the charging and discharging processes. A low charge transfer resistance (with R_{ct} being 64.18 Ω) reveals that the charge transfer process at the electrode/electrolyte interface of the device is relatively easy, which has a positive impact on the rapid occurrence of electrochemical reactions. Subsequently, the actual capacitance performance of the device was tested by CP measurements (Fig. 4c). The capacitance reached a satisfactory value of 46 F g^{-1} (at 1 A g^{-1}). Moreover, the capacitance exhibited only a 28.6% attenuation (at 10 A g^{-1}) and reached 33 F g^{-1} (Fig. 4d), which demonstrated that the device exhibited excellent rate performance. When testing the capacitance stability (Fig. 4e), it was found that the capacitance retention rate reached 75% after 3000 cycles, indicating that the device had excellent cycling stability. The excellent energy density (9.1 W h kg^{-1}) and good power density (595.6 W kg^{-1}) of the device were calculated. The ultraviolet absorption spectra within the voltage range of 0–1.2 V are scanned (Fig. 4f). It was observed that there are significant

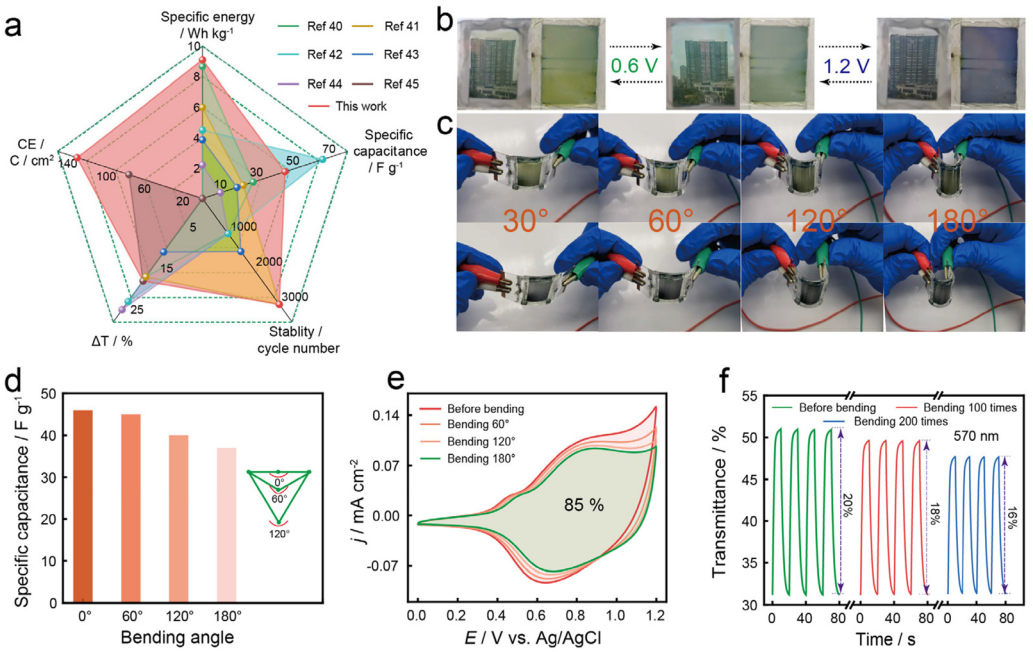

Fig. 5 Application of patterned **PHTPA**-based flexible EC-SC devices. (a) Radar chart of the key performance comparison for flexible devices. (b) Device-simulated electrochromic windows under different voltages. (c) Color variations of the device under different bending angles. (d) Capacitance values of the device being tested under different bending angles. (e) CV curves of the device being tested under different bending angles. (f) Transmittance curves of the device being tested after different bending times.

differences in the ultraviolet absorption at 430 nm and 570 nm. Furthermore, the transmittance switching curves of the device were tested (Fig. 4g). The transmittance at 430 nm and 570 nm reached 16% and 20% respectively. The coloring efficiency of the device at 570 nm was calculated to be 130.1 C cm^{-2} (Fig. 4h) according to the following formula. A high coloring efficiency indicates that the device possesses a favorable charge utilization efficiency and can effectively reduce energy consumption in practical applications.

$$CE = \frac{\Delta OD}{\Delta Q} = \log\left(\frac{T_b}{T_c}\right)/\Delta Q$$

ΔQ denotes the accumulated charge of the working electrode at the applied voltage. T_b and T_c are the transmission values at specific wavelengths for the coloring and bleaching states, respectively.[38,39] The chronoamperometry test was carried out on the device for a long period (with a pulse time of 10 s) to evaluate the electrochromic stability of the device (Fig. 4i). The results showed that after 5000 s of cycling, the transmittance at 570 nm remained at 70%, and the device still exhibited obvious color changes. All in all, the flexible EC-SC devices assembled based on **PHTPA** films simultaneously demonstrate excellent specific capacitance and conspicuous color changes, exhibiting outstanding comprehensive performance. Moreover, the devices still exhibit obvious color variations.

3.5. Practical applications of flexible devices

A comparison of the key performance between our work and previous studies was conducted (Fig. 5a).[40–45] It was conspicuously found that our device exhibited excellent comprehensive performance (including high energy density capacitance, large coloring efficiency and long-term stability), which further verified the practical application potential of this device. Electrochromic windows were simulated using the device (Fig. 5b). The device changed from green to blue within the voltage range of 0–1.2 V. The conspicuous color change avoided the light pollution issue caused by transparent glass, thus showing tremendous application potential in architectural glass and automobile rearview mirrors. In order to explore the application value in multiple scenarios, a series of bending tests were carried out on the device. Under different bending angles (ranging from 30° to 180°), the device still maintained excellent color-changing ability (Fig. 5c) and a capacitance retention rate of 80% (Fig. 5d). Moreover, the active area of the CV curve even remained at 85% (Fig. 5e). After being repeatedly bent (with a bending radius of 60°) for 200 times, there was only a 20% attenuation in the transmittance (at 570 nm) (Fig. 5f). The above experimental results have verified that the device possesses excellent mechanical flexibility.

4. Conclusion

In summary, we propose a design approach centered around conjugated extended structures for the fabrication of novel high-performance **PHTPA** EC-SCs. The relatively expansive conjugated structures fortify the π–π stacking effect and furnish an increased number of active sites. This enables the synthesized **PHTPA** film to manifest excellent electrochromic properties (ΔT reaches 51% at 1050 nm), while concurrently demonstrating commendable capacitive capabilities (177 F g^{-1} at 1 A g^{-1}). Based on this, a flexible EC-SC device was fabricated using the **PHTPA** film, which not only exhibits a high specific capacitance (46 F g^{-1} at 1 A g^{-1}) but also displays distinct color alterations and remarkable bending resistance. The design strategy of conjugated extended structures, along with the high-performance **PHTPA** film, holds great promise in propelling the development of reliable flexible EC-SCs across diverse fields, including intelligent energy storage and flexible wearable electronics.

Author contributions

Jiaming Li and Xu Cheng were responsible for experimental data processing, analysis, and manuscript writing. Wenyuan Xu, Li Sheng, and Wanyi Zhang participated in the writing of specific sections and conducted a comprehensive review and revision of the manuscript. Xubiao Luo, Ge Zhang, Hui Shi, and Chunhui Du reviewed and revised the manuscript. All authors contributed to the article and approved the submitted version.

Data availability

The data supporting this article are included in the ESI.†

Conflicts of interest

The authors declare no conflicts of interest.

Acknowledgements

We are grateful to the National Natural Science Foundation (52364039, 52103214 and 52373184), the Jiangxi Provincial Natural Science Foundation (GJJ2201301 and 20242BAB23025), the Scientific Fund of Jiangxi Science & Technology Normal University (2022QNBJRC004), and the Jiangxi Provincial Key Laboratory of Flexible Electronics (20242BCC32010).

References

1 D. Pandey, K. S. Kumar and J. Thomas, *Prog. Mater. Sci.*, 2024, **141**, 101219.
2 B. Chettiannan, E. Dhandapani, G. Arumugam, R. Rajendran and M. Selvaraj, *Coord. Chem. Rev.*, 2024, **518**, 216048.

3 J. Mitali, S. Dhinakaran and A. A. Mohamad, *Energy Storage Sav.*, 2022, **1**, 166–216.
4 T. G. Yun, X. Chen and J. Y. Cheong, *Batteries Supercaps*, 2023, **6**, e202200454.
5 R.-T. Ginting, M.-M. Ovhal and J.-W. Kang, *Nano Energy*, 2018, **53**, 650–657.
6 S. Kandpal, T. Ghosh, C. Rani, A. Chaudhary, J. Park, P. S. Lee and R. Kumar, *ACS Energy Lett.*, 2023, **8**, 1870–1886.
7 X. Chen, Q. Liu, L. Cheng, S. Zhou, L. Chen, G. Liang, J. Wei and F. Mo, *Adv. Mater. Technol.*, 2024, **9**, 2301969.
8 S. Halder and C. Chakraborty, *Nano Energy*, 2024, **131**, 110243.
9 Q. Liu, L. Yang, W. Ling, B. Guo, L. Chen, J. Wang, J. Zhang, W. Wang and F. Mo, *Front. Chem.*, 2022, **10**, 1001425.
10 J. Wang, X. Huo, M. Guo and M. Zhang, *J. Energy Storage*, 2022, **47**, 103597.
11 F. Zhao, B. Wang, W. Zhang, S. Cao, L. Liu, A. Y. Elezzabi, H. Li and W. W. Yu, *Mater. Today*, 2023, **66**, 431–447.
12 B. Cong, Y. Xie, Y. Wu, H. Zhou, C. Chen, X. Zhao and D. Chao, *Chem. Eng. J.*, 2023, **474**, 145528.
13 E. G. C. Ergun and A. M. Önal, *J. Energy Storage*, 2024, **104**, 114512.
14 Y. Zhang, F.-Q. Bai, Y. Xie, M. Zhu, L. Zhao, D. An, D. Xue, E. B. Berda, C. Wang, G. Lu, X. Jia and D. Chao, *Chem. Eng. J.*, 2022, **450**, 138386.
15 E. G. C. Ergun and A. M. Önal, *Electrochim. Acta*, 2025, **510**, 145379.
16 M. Gao, J. Wu, X. Yuan, C. He, H. Jiang, W. Zhao, C. Duan, Y. Chen, Y. Ke, H. Yao and L. Ye, *Energy Environ. Sci.*, 2023, **16**, 5822–5831.
17 K. Janus, D. Chlebosz, A. Janke, W. Goldeman and A. Kiersnowski, *Macromolecules*, 2023, **56**, 964–973.
18 N. Li, Y. Y. Wang, W. D. Zhao, Z. H. Chen, P. P. Liu, W. Q. Zhou, F. X. Jiang, C. C. Liu and J. K. Xu, *ChemPhysChem*, 2024, **25**, e202400103.
19 H. Han, J. S. Lee and S. Cho, *Polymers*, 2019, **11**, 232.
20 S. Nie, Z. Li, Z. Su, Y. Jin, H. Song, H. Zheng, J. Song, L. Hu, X. Yin, Z. Xu, Y. Yao, H. Wang and Z. Li, *ChemSusChem*, 2023, **16**, e202202208.
21 M. Mladenovic and N. Vukmirovic, *Adv. Funct. Mater.*, 2015, **25**, 1915–1932.
22 S. Xue, Y. Sun, J. Cao, H. Lin, X. Zang and S. Chen, *Electrochim. Acta*, 2022, **423**, 140575.
23 Y. Wang, X. Wang, X. Li, Y. Bai, H. Xiao, Y. Liu, R. Liu and G. Yuan, *Adv. Funct. Mater.*, 2019, **29**, 1900326.
24 J. Tao, H. Chen, Y. Han, L. Pu, X.-P. Zhang, S. Peng, Z. Wu, H. Liu and J. Liu, *Polymer*, 2023, **285**, 126386.
25 Y. Zhuang, W. Zhao, L. Wang, F. Li, W. Wang, S. Liu, W. Huang and Q. Zhao, *Sci. China: Chem.*, 2020, **63**, 1632–1644.
26 Y. Pan, P. Gao, H. J. Chen, X. P. Zhang, Y. Y. Han, Z. Gu, J. K. Xu, R. Zhang and J. Liu, *J. Mol. Struct.*, 2023, **1292**, 136182.
27 M. Shao, X. Lv, C. Zhou, M. Ouyang, X. Zhu, H. Xu, Z. Feng, D. S. Wright and C. Zhang, *Sol. Energy Mater. Sol. Cells*, 2023, **251**, 112134.
28 R. Wang, J. Li, L. Gao and J. Yu, *Chem. Eng. J.*, 2022, **445**, 136731.
29 S. Ming, S. Zhen, H. Zhang, Z. Zhang, B. Lu, J. Zhao, G. Nie and J. Xu, *Polymer*, 2023, **267**, 125675.
30 Q. Huang, J. Chen, X. Shao, L. Zhang, Y. Dong, W. Li, C. Zhang and Y. Ma, *Chem. Eng. J.*, 2023, **461**, 141974.
31 X. Lv, J. Li, L. Zhang, M. Ouyang, A. Tameev, A. Nekrasov, G. Kim and C. Zhang, *Chem. Eng. J.*, 2022, **431**, 133733.
32 Y. Xie, Y. Zhang, M. Zhu, R. Huang and D. Chao, *Dyes Pigm.*, 2023, **208**, 110889.
33 D. Jhankal, M. S. Khan, K. K. Jhankal and K. Sachdev, *J. Phys. Chem. Solids*, 2023, **173**, 111117.
34 B. Wang, J. Li, M. Ye, Y. Zhang, Y. Tang, X. Hu, J. He and C. C. Li, *Adv. Funct. Mater.*, 2022, **32**, 2112072.
35 A. M. Teli, S. A. Beknalkar, R. U. Amte, P. J. Morankar, M. A. Yewale, V. V. Burungale, C.-W. Jeon, H. Efstathiadis and J. C. Shin, *J. Alloys Compd.*, 2023, **965**, 171305.
36 D. Bessinger, K. Muggli, M. Beetz, F. Auras and T. Bein, *J. Am. Chem. Soc.*, 2021, **143**, 7351–7357.
37 Y. Han, Z. Xing, P. Ma, S. Li, C. Wang, Z. Jiang and Z. Chen, *ACS Appl. Mater. Interfaces*, 2020, **12**, 7529–7538.
38 Z. Shao, A. Huang, C. Ming, J. Bell, P. Yu, Y.-Y. Sun, L. Jin, L. Ma, H. Luo, P. Jin and X. Cao, *Nat. Electron.*, 2022, **5**, 45–52.
39 R. Li, X. Ma, J. Li, J. Cao, H. Gao, T. Li, X. Zhang, L. Wang, Q. Zhang, G. Wang, C. Hou, Y. Li, T. Palacios, Y. Lin, H. Wang and X. Ling, *Nat. Commun.*, 2021, **12**, 1587–1598.
40 C.-H. Du, Y.-H. Xu, H. Li, Z.-X. Wu, H.-J. Yang, X.-M. Liu, B.-Y. Lu, G.-M. Nie and G. Zhang, *Chin. J. Polym. Sci.*, 2024, **42**, 1749–1757.
41 C. Du, H. Li, G. Zhang, R. Wan, W. Zhang, X. Xu, L. Zheng, X. Deng, J. Xu, B. Lu and G. Nie, *Chem. Eng. J.*, 2024, **495**, 153692.
42 H. Li, J. Cao, F. Liu, W. Zhou, X. Chen, Y. Deng, Z. Wu, B. Lu, D. Mo, J. Xu and G. Zhang, *ACS Appl. Energy Mater.*, 2022, **5**, 12315–12323.
43 W. Zhang, J. Cao, H. Li, C. Du, S. Chen, L. Cao, J. Xu, B. Lu and G. Zhang, *J. Energy Storage*, 2024, **98**, 113154.
44 O. Eisenberg, Y. M. Algavi, H. Weissman, J. Narevicius, B. Rybtchinski, M. Lahav and M. E. van der Boom, *Adv. Mater. Interfaces*, 2020, **7**, 2000718.
45 Y. Li, L. Yan, L. Zhang, X. Song and C. Dai, *J. Mater. Sci.: Mater. Electron.*, 2021, **32**, 19179–19190.